The Astrophysical Journal, 875:146 (11pp), 2019 April 20 https://doi.org/10.3847/1538-4357/ab0d8f

Scattering Study of Pulsars below 100 MHz Using LWA1

K. Bansal[1], G. B. Taylor[1], Kevin Stovall[2], and Jayce Dowell[1]
[1] Department of Physics and Astronomy, University of New Mexico, Albuquerque, NM 87131, USA
[2] National Radio Astronomy Observatory, Socorro, NM, USA
Received 2018 November 26; revised 2019 March 4; accepted 2019 March 5; published 2019 April 24

Abstract

Interstellar scattering causes pulsar profiles to grow asymmetrically, thus affecting the pulsar timing residuals, and is strongest at lower frequencies. Different interstellar medium models predict different frequency (ν) and dispersion measure (DM) dependencies for the scattering timescale τ_{sc}. For Gaussian inhomogeneity the expected scaling relation is $\tau_{sc} \propto \nu^{-4}$ DM^2, while for a Kolmogorov distribution of irregularities, the expected relation is $\tau_{sc} \propto \nu^{-4.4}$ DM$^{2.2}$. Previous scattering studies showed a wide range of scattering index across all ranges of DM. A scattering index below 4 is believed to be either due to limitations of the underlying assumptions of the thin-screen model or an anisotropic scattering mechanism. We present a study of scattering for seven nearby pulsars (DM < 50 pc cm^{-3}) observed at low frequencies (10–88 MHz), using the first station of the Long Wavelength Array. We examine the scattering spectral index and DM variation over a period of about three years. The results yield insights into the small-scale structure of the interstellar medium, as well as the applicability of the thin-screen model for low-DM pulsars.

Key words: ISM: general – pulsars: general

1. Introduction

The interstellar medium (ISM) consists of an ionized and turbulent plasma that causes a delay in time and variations in the phase of radio signals. The subsequent interference gives rise to a diffraction pattern and broadens the apparent size of a source. Some observable ISM effects are dispersion, scattering, angular broadening, and interstellar scintillation. The dispersion causes a delay between the pulse arrival times of the upper and lower ends of a broadband pulsar signal. The scattering of a pulse signal causes temporal broadening, making average profiles grow asymmetrically broader at lower frequencies (e.g., Lohmer et al. 2001, 2004; Lewandowski et al. 2013, 2015). Pulsars are compact sources and emit short periodic pulses, making them good sources for studying and understanding these propagation effects.

Assuming that the scattering occurs due to a thin screen between the observer and the source, the pulse-broadening function can be expressed in terms of an exponential function $\sim\exp(-t/\tau_{sc})$ with scattering parameter τ_{sc} (Scheuer 1968). This is also known as the thin-screen model, where different ISM models of electron density fluctuations predict different frequency dependencies for the scattering parameter given by $\tau_{sc} \propto \nu^{-\alpha}$, where α is the scattering time spectral index. This model considers an isotropic homogeneous turbulent medium. For Gaussian inhomogeneity (Lang 1971), the scaling relation is

$$\tau_{sc} \propto \nu^{-4}\mathrm{DM}^2, \tag{1}$$

while for a purely Kolmogorov distribution of inhomogeneities (Romani et al. 1986), the expected relation is

$$\tau_{sc} \propto \nu^{-4.4}\mathrm{DM}^{2.2}. \tag{2}$$

In both Equations (1) and (2), ν and dispersion measure (DM) are frequency and DM, respectively. The DM is given by $\int n_e dl$, where n_e is the electron density and dl is the path length along the line of sight (LOS). Measurements of DM have helped us understand the distribution of free electrons and estimate pulsar distances in our Galaxy (Cordes & Lazio 2002; Yao et al. 2017).

The amount of observed scattering can be estimated by assuming a spectrum of electron density fluctuations. A simple power-law model is given by

$$P_{ne}(q) = C_{ne}^2 q^{-\beta}, \tag{3}$$

where q is the amplitude of a three-dimensional wavenumber and C_{ne}^2 is the fluctuation strength along a given LOS. The above simplification is valid when the inverse of wavenumber q ($1/q$) is much larger than the inner scale, and much lower than the outer scale (Lambert & Rickett 1999). The value of β ranges between 2 and 4 and is related to the scattering spectral index via

$$\alpha = \frac{2\beta}{(\beta - 2)}. \tag{4}$$

This simplified version of the scattering strength (Equation (3)) may not be valid for real cases, which are difficult to predict because we do not have information about the inner/outer scales. When the diffractive scale drops below the inner scale, the dependence becomes quadratic. This change in diffractive scale with observing frequency leads to flatter spectra in comparison to the theoretical value at lower frequencies (see Rickett et al. 2009; Lewandowski et al. 2015).

In previous scattering studies, while the average value of α seems to agree with the theoretical models, for individual pulsars, large deviations have been detected across all ranges of DM (Lewandowski et al. 2015). For large DMs (>300 pc cm^{-3}), Lohmer et al. (2001) reported a mean value for α of 3.400 ± 0.013 obtained from frequencies between 600

Table 1
List of the Sources Studied in This Paper

Selected Pulsars Observed with LWA1					
Source	DM_{LWA1} (pc cm^{-3})	Period (s)	Distance (kpc)	$PM_{R.A.}$ (mas yr^{-1})	$PM_{decl.}$ (mas yr^{-1})
B0329+54	26.7639(1)	0.71452	1.00	17.0(0.3)	−9.5(0.4)
B0823+26	19.4789(2)	0.5307	0.32	61.0(3)	−90.0(3)
B0919+06	27.2986(5)	0.4306	1.10	18.8(.9)	86.4(0.7)
B1822−09	19.3833(9)	0.7690	0.30	−13(11)	−9(5)
B1839+56	26.774(1)	1.6529	2.19	−30(4)	−21(2)
B1842+14	41.498(1)	0.3755	1.68	−9(1)	45(1)
B2217+47	43.488607(5)	0.5385	2.39	−12(8)	−30(6)

Note. DM and period values have been obtained from Stovall et al. (2015). Values for the distance, $PM_{R.A.}$, and $PM_{decl.}$ have been obtained from the ATNF (http://www.atnf.csiro.au/people/pulsar/psrcat/) pulsar catalog.

MHz and 2.7 GHz. The authors explained that this could be due to the presence of multiple screens between the pulsar and the observer. Lewandowski et al. (2013, 2015) reported α in the range of 2.61–5.61, obtained for a sample of 60 pulsars. They also see α values below 2.61, but discarded them due to poor data quality. Geyer & Karastergiou (2016) simulated anisotropically scattered data and fit them with the isotropic model, which resulted in α values less than the theoretically predicted values, as well as the effect of non-circular scattering screens leading to low α values ($\sim$2.9). Scattering spectra with $\alpha < 4$ have been interpreted as a limitation of the assumptions underlying the thin scattering model. Plausible deviations from the thin-screen assumptions include a truncated scattering screen (Cordes & Lazio 2001), the impact of an inner cutoff scale (Rickett et al. 2009), and anisotropic scattering mechanisms (Stinebring et al. 2001).

Moreover, ISM scattering accounts for one of the largest time-varying sources of noise in timing residuals of pulsars, which are used by pulsar timing arrays (PTAs) to detect gravitational waves from supermassive binary black holes (for more details see Ferdman et al. 2010; Shannon et al. 2015; Arzoumanian et al. 2018). Despite pulsars exhibiting steep spectra that imply higher flux at lower frequencies (Seiber 1973), a large population of pulsars at lower frequencies is marginalized from the PTA analysis, where dispersion and scattering effects are greatest. These reasons further motivate us to undertake a study of propagation effects with pulsars at low frequencies. In this paper we focus on the scattering effects for a sample of pulsars observed at low frequencies (10–88 MHz), using the first station of the Long Wavelength Array (LWA1). We examine the scaling relations for scattering with time and frequency. We model for both the frequency dependence of the scattering time as well as the DM, as α depends on both.

This paper has been organized in the following manner. In Section 2 we describe our observations and preliminary data reduction. In Section 3, we describe the scattering analysis methods. In Section 4, we describe the results for our sample of seven pulsars. Section 5 contains a detailed discussion and comparison with previous observations.

2. Observations

The LWA1 (Taylor et al. 2012) is a radio telescope array located near the Karl G. Jansky Very Large Array in central New Mexico. It consists of 256 dual-polarized dipole antennas operating in the frequency range 10–88 MHz. The outputs of the dipoles can be formed into four fully independent dual-polarization beams such that each beam has two independent frequency tunings (chosen from the range 10–88 MHz) with a bandwidth of up to 19.6 MHz in each tuning. The ability of the LWA1 to observe multiple frequencies simultaneously provides a powerful tool for studying the frequency dependence of pulsar profiles (Ellingson et al. 2013). At these low frequencies, the pulses experience scattering and dispersion effects to a much greater extent than at higher frequency. Thus, the LWA1 can be used to make very precise measurements of these effects for studying the ISM properties.

The LWA Pulsar Data Archive[3] (Stovall et al. 2015) contains reduced data products for over 100 pulsars (K. Stovall et al. 2019, in preparation) observed since 2011. The data products used for this study are produced by coherently dedispersing and folding the raw LWA data using DSPSR.[4] We used archival observations at four frequency bands: 35.1, 49.8, 64.5, and 79.2 MHz. The archival data have already been corrected for DM effects via coherent dedispersion, and consist of 4096 phase bins for each of 512 spectral channels. The data are saved in the form of 30 s sub-integrations.

We excise RFI using a median zapping algorithm that removes data points with intensity more than six times compared to the median within a range of frequency channels. These files are then further reduced in two ways; one is to obtain total average profiles with two to four channels (depending on the signal-to-noise ratio (S/N) of a pulsar) for scattering studies and the other with eight channels is to obtain the pulse time of arrivals (TOAs) for measuring the DM variation over time. For scattering study, we reduce the number of phase bins to 256 to smooth the average profiles. These tasks are performed using the PSRCHIVE command `pam` (van Straten et al. 2012). We also remove the baseline from the observed profiles and then normalize them by their peak amplitude.

In our preliminary study of scattering, we obtain archival data for seven pulsars (Table 1) for all the available epochs since the commission of LWA1. For each pulsar, we split each frequency band into two channels, except for two pulsars: PSR B1822−09 and PSR B1839+56. For PSR B1822−09 we have used four channels to compare our results with previous studies by Krishnakumar et al. (2015). In case of PSR B1839+56, we have reduced the data to four channels to improve our sample size, as the S/N at higher-frequency bands (64.5 and 79.2

[3] https://lda10g.alliance.unm.edu/PulsarArchive/
[4] http://dspsr.sourceforge.net/index.shtml

Table 2
IPM Frequency Parameters

Pulsar	Epoch Range MJD	Number of Gaussian Components	Frequencies Used (MHz)	Frequency Dependence (a, b)
B0329+54	57144–58254	4	40.0, 44.9, 54.7 59.6, 69.4, 74.3	0.00655, −0.0811
B0823+26	57219–57899	2	44.9, 54.7, 59.6 69.4, 74.3	...
B0919+06	57312–58139	3	44.9, 54.6, 59.6 69.4, 74.3	...
B1822–09	57232–57919	1	47.3, 52.2, 57.2 62.0, 67.0, 71.8	0.0188, −0.166
B1839+56	57225–58209	1	27.8, 32.6, 37.6 42.4, 47.4, 52.2 57.2, 62.0	...
B1842+14	57242–58210	2	49.7, 59.6, 69.4 74.2, 84.1	0.461, −0.917
B2217+47	57242–58085	1	44.9, 54.6, 59.6, 69.4, 74.3, 84.1	0.127, −0.602

Note. This table lists the range of epochs that have been included in this study for each pulsar, the number of Gaussian components, the frequencies used for each pulsar, and the frequency modeling parameters for the main component width to obtain the IPM given by $a \times \nu^b$ (discussed in Section 3.1).

MHz) is poor. The analyzed frequency range was cut for all the pulsars with regard to full LWA capabilities due to S/N issues coming from the shape of pulsar spectra and/or sensitivity. We list the center frequencies used for each pulsar in Table 2.

These seven pulsars were previously noted to have profile shapes below 100 MHz that are consistent with the effects of interstellar scattering (Stovall et al. 2015) and we follow the same data reduction procedure for all of them (see Section 3).

3. Analysis

After obtaining the average profiles for each pulsar, we follow the same technique reported in Krishankumar et al. (2015, hereafter, KK15) to model scattering on this data set. This formulation is based on the simple thin-screen model (Williamson 1972). The observed pulse profile can be expressed as a convolution of the frequency-dependent intrinsic pulse $P_i(t, \nu)$ with the impulse response, characterizing the pulse scatter broadening in the ISM, $s(t)$ the dispersion smear across the narrow spectral channel $D(t)$, and the instrumental impulse response, $I(t)$. This results in $P(t) = P_i(t, \nu) * s(t) * D(t) * I(t)$, where $*$ denotes convolution. Following the same analysis as in KK15, we ignore the effect of $I(t)$, as our instrument is stable in time on the timescale of each observation. $D(t)$ can also be ignored, as we use coherent dedispersion that corrects for dispersion smearing in the narrow spectral channel.

3.1. Intrinsic Pulse Model

The average pulse profile of a pulsar varies intrinsically with frequency in the number of components, their width, amplitude ratio, and separation between them. Hence, it is important to account for frequency-dependent effects. Since the intrinsic pulse profile of a pulsar is unknown, we obtain an expected intrinsic profile model (IPM) at our frequency of interest using higher-frequency average profiles for each source in Table 1. We assume the effects of scattering at higher frequencies are too small to affect the pulse shape. Average profiles at multiple frequencies enable us to obtain frequency-dependent variation in the parameters affecting the pulse shape. For the IPM, we obtain average pulse profiles at frequencies ranging between ∼100 and 410 MHz from the European Pulsar Network (EPN[5]). However, if one of the profiles in the above frequency range has poor S/N or two average profiles are close in frequency (143 and 151 MHz), it is difficult to accurately determine the frequency evolution. In such cases, we either consider no frequency evolution (see Table 2) or include our 79.2 MHz data (highest central frequency in the LWA1 band) depending on its S/N. Differences in these average profiles apart from the intrinsic frequency effects of interest can also stem from different telescopes, instrumentation, observation date, and duration.

We model these profiles using a sum of Gaussians as explained in Kramer (1994). The number of Gaussian components increases with each iteration and is limited to a maximum of five. We use various criteria to limit the number of Gaussian components; for example, the iteration stops when the amplitude of the residual maxima is <5% of maximum peak intensity or the chi-squared value increases with the addition of a new Gaussian component.

We assume that the number of components does not change within the selected range of frequencies (79.2–410 MHz). Once we obtain a set of Gaussian parameters for a profile at one of the frequencies (preferably LOFAR high band since it offers high S/N), we use these parameters as an initial condition and apply them to rest of the frequency profiles. We then fit for changes in the main component width based on a power law in frequency (for the list of parameters, see Table 2), as pulsars have broader pulse profiles at lower frequencies (Lyne & Graham-Smith 2006). We also assume that spacing between the components and their relative amplitudes do not vary within our frequency selection. We consider the radius-to-frequency mapping only for the pulse width. Two pulsars (PSR B0329+54 and PSR B0919+06) in our sample have more than two components, which makes determining the evolution of the component separation very complicated. In order to have a consistent analysis we refrain from applying radius-to-frequency mapping for the remaining pulsars.

[5] http://www.epta.eu.org/epndb/

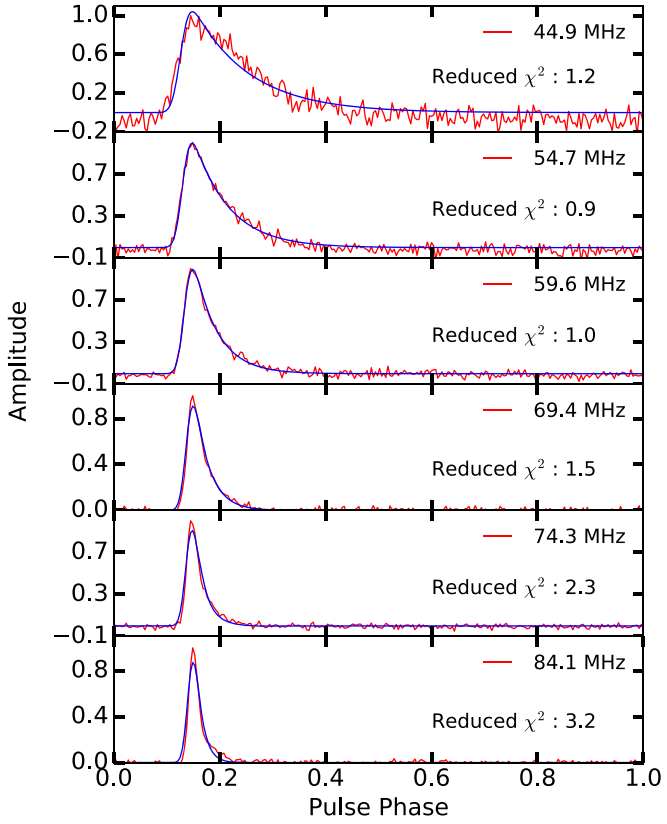

Figure 1. Fitting example for B2217+47 epoch MJD 57372. From top to bottom the plots show fittings of intrinsic pulse models convolved with an exponential scattering function to the observed data. For B2217+47, the noise in the data increases as we go toward the lower frequencies.

3.2. Pulse Broadening

From the high-frequency models described above, we derive the frequency dependence and a new IPM is obtained for all the LWA1 center frequencies separately. The IPM is convolved with an exponential function with a scattering time (τ_{sc}) to obtain a template. This new template is a function of relative flux, phase offset, and scattering timescale. We then use a least square fitting algorithm to fit the template to the observed pulse profiles. This fitting uses the standard deviation of observed pulse profile as the uncertainty and estimates error bars on the fitting parameters. We assume that error on the template is negligible compared to the uncertainty in the data and will not affect the fitting parameters. To align the pulse phase of the template and data, we use a low-pass filtering technique to smooth the data. To do this, we first calculate the Fourier transform of the average profile. Then we filter out all the frequencies >30% of the maximum frequency (fmax) and rescale the intensities for frequencies between 20% and 30% of fmax by $(N - n_i)/N$, where n_i is the index of the frequency point and N is the total number of points within the specified frequency range. Intensities at frequency <10% of the fmax are scaled by 1. We include these two frequency ranges to avoid sharp edges. We then take the inverse Fourier transform of the filtered profile and use that to find the peak location. Since this filters out all the high Fourier frequencies, noise interferes less with determining the phase of the peak.

We plot the fitting examples for PSR B2217+47 at all six frequencies in Figure 1 to demonstrate our procedure. As can be seen, our templates (Figure 1) fit the observed data set with a reduced chi-square in the range of 1–3 for all frequencies. Subsequently, we use τ_{sc} obtained from Figure 1 to obtain an α value for PSR B2217+47 (Figure 2). Similarly, we have obtained an IPM for all the pulsars in our sample and used them to fit our observations.

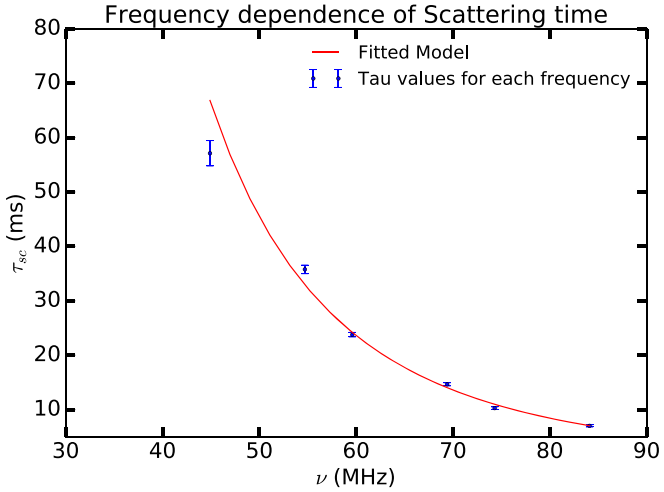

Figure 2. Example of an α fit for PSR B2217+47 at epoch MJD 57372.

3.3. DM Variation

Since the scattering time can be related to DM (see Equations (1) and (2)) along the LOS, it is important to study if there are any variations in DM over the duration of our observations. For our study, we measure δDM using the pulsar timing software TEMPO[6] DMX parameters. These measure an offset of DM from a fiducial value for multiple epochs each having a specified time span. We used a time span of about three years.

For the DM analysis, the number of frequency channels in the archive files is reduced to eight for each epoch at two frequencies, 64.5 and 79.2 MHz, using the PSRCHIVE task pam. We only use the higher frequencies because they have a better S/N. The TOAs for these profiles are obtained using pat (a PSRCHIVE algorithm). For the timing model, we first apply ephemeris changes using the task pam to make sure all of the epochs have the same ephemeris, and then average profiles across all the epochs for each frequency using psradd, followed by smoothing the profile using psrsmooth. We then align the 64.5 and 79.2 MHz pulse models, before obtaining the TOAs. We have converted the TOAs to the solar system barycenter using the DE405 model (Standish 1998). The time difference between the observed TOA and the timing model gives timing residuals for each observation. We combine these timing residuals from both the frequencies into one file and fit for the above-listed parameters.

4. Results

We have studied scattering in seven pulsars using the LWA1 data. Below we discuss our results for each pulsar individually.

4.1. PSR B0329+54

PSR B0329+54 is known to have nine emission components, one of the highest number of components for any pulsar

[6] http://tempo.sourceforge.net/

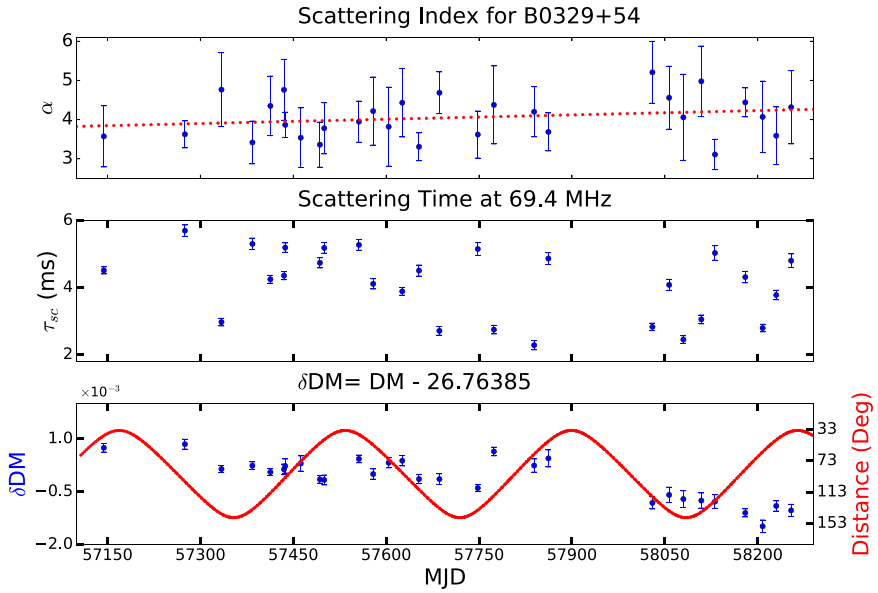

Figure 3. The top and middle panels consist of scattering index values (α) and scattering time at 69.4 MHz, respectively, over time for PSR B0329+54. The bottom panel consists of δDM values (blue) and solar elongation angle (red) over time. All four measurements have been made at the same epochs for a span of about three years. For more details see Section 3.

(Gangadhara & Gupta 2001). We have used four components where the amplitude of these components is above 5% of the main component amplitude. The frequency evolution for the main component has been obtained from three frequencies: 79.2, 143, and 408 MHz (obtained from EPN).

We have plotted α, τ_{sc}, δDM, and the solar elongation angle in Figure 3. The measured median α value is 4.05 ± 0.14. This estimate is in agreement with the prediction of the Gaussian distribution where the α value is expected to be 4.0. The fitting to the α value over time yields a slope equal to $0.13 \pm 0.11\ \mathrm{yr}^{-1}$. This is consistent with there being little or no variation in the scattering index with time.

PSR B0329+54 has been found to have periodic variation in its timing residuals, with two different periods likely due to the presence of potential planets (Starovoit & Rodin 2017) in its orbit. This contributes to the timing noise, hence we have obtained the DM values for this pulsar in a slightly different manner. Instead of fitting for δDM across all epochs simultaneously, we have fit for each epoch individually. Figure 3(b) shows the variation in δDM values with an overall change of about $0.0015\ \mathrm{pc\ cm}^{-3}$ over a span of about 3 yr. These variations do not correlate with the solar elongation angle (Figure 3(c)) where the trend is periodic. We do not expect this pulsar to exhibit variation in DM due to the solar wind because the closest distance of approach is 34.2°. This pulsar is also known to exhibit mode switching (Chen et al. 2011), where the relative amplitude of the component changes and the total pulse width becomes narrower as the profile components change their phases. These mode changes are simultaneous across frequency but non-uniform (Bartel et al. 1982), hence we will introduce a frequency-dependent variation in timing residuals. Apart from mode change, it is also known to have planets in its orbit that will again affect the timing residuals. Hence, this apparent variation in δDM is not due to any physical change in ISM, but instead due to the high timing noise of this pulsar.

4.2. PSR B0823+26

The PSR B0823+26 pulse profile consists of a main pulse, post-cursor, and an inter-pulse (Rathnasree & Rankin 1995). The amplitude of both the inter-pulse and post-cursor is less than 5% of the main pulse. However, we note there are two additional wing components on both sides of the main pulse that are above 5% of the main pulse's amplitude at 143 and 151 MHz. It is difficult to obtain frequency dependency from only these two nearby frequencies, especially when it involves multiple components. Hence, for the IPM, we have used the profile at 151 MHz and considered no frequency evolution.

This pulsar is known to exhibit nulling, detected in LOFAR observations (Sobey et al. 2015), which causes several observations without any pulse, hence they have been excluded from this analysis. We have plotted the α and DM values over time in the top and bottom panels of Figure 4, respectively. The estimated median α value for this pulsar is 1.55 ± 0.09, which is quite small in comparison to the expected theoretical value. We fit a trend to the α values over time and have found the slope value to be $-0.16 \pm 0.13\ \mathrm{yr}^{-1}$. This is consistent with there being little or no variation in the scattering index over time.

From the δDM plot (Figure 4(b)), we see a periodic variation of $\sim 1.7 \times 10^{-3}\ \mathrm{pc\ cm}^{-3}$ over a period of about half a year. This periodicity in DM can be attributed to the solar wind, due to its close proximity to the Sun (Figure 4(c)). The closest distance of approach for this pulsar is about 7°.

4.3. B0919+06

The number of components in B0919+06 is a matter of some debate because this pulsar is known to exhibit abnormal emission that causes flares a few degrees in phase before the normal emission (Rankin et al. 2006; Han et al. 2016). The timescale of this emission is about 15 s and expected to occur once in 1000 pulses. Since for our analysis we average an hour-long archival observation in time, we do not detect it. The Gaussian fitting of the 135 MHz profile yields three

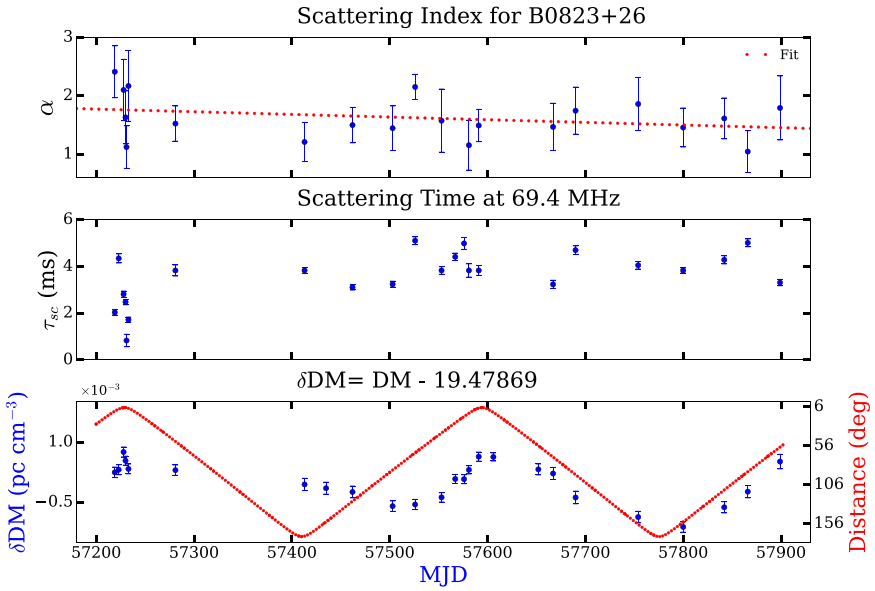

Figure 4. α, τ_{sc} at 69.4 MHz, δDM, and solar elongation angle for every epoch for PSR B0823+26.

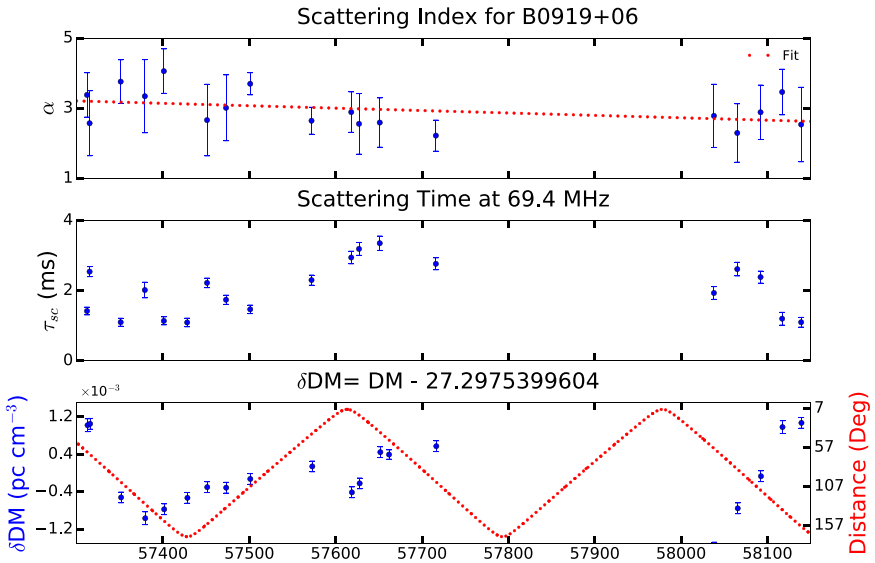

Figure 5. α, τ_{sc} at 69.4 MHz, δDM, and solar elongation angle for every epoch for B0919+06.

components and the 408 MHz profile shows only two components, where the post-cursor component is missing. Due to this we only derive the IPM from 135 MHz with no frequency evolution. The value 135 MHz is closer to the frequencies we are working with compared to 408 MHz, which is six times larger. This provides the best possible fits for this pulsar.

The average α value is 2.88 ± 0.18. The slope value is $-0.28 \pm 0.15\,\mathrm{yr}^{-1}$. The epochs ranging from MJD 57744 to 57903 either have poor data quality or a smaller number frequencies, hence they have not been included in the fitting plot. For B0919+06, the scattering time ($\sim$5 ms) is small in comparison to PSR B2217+47 and B0329+49 ($\sim$30 ms) at the frequencies of LWA1. This could imply that pulsars with similar DM values (PSR B0329+54) have different scattering timescales, as it also depends on the location of a source in the galaxy.

This pulsar appears to have a steep spectrum at the LWA frequencies and consequently the S/N deteriorates when we go toward the higher end of the spectrum. Hence, we ignore the last channel (84.1 MHz) for scattering index estimation. For some of the epochs, the average profile fits poorly with the model for the mid-range frequencies and we get a lower scatter timescale for a higher frequency. It seems that this may be attributed to the error in τ_{sc} and these error bars may be underestimated.

The δDM plot (Figure 5(c)) exhibits variation over time, with no overall change in δDM value. The minimum solar elongation angle for this pulsar is 8.36°. Thus, we expect the variation in δDM due to the solar winds (Figure 5(c)) to be periodic, which does not align with our δDM observations. This pulsar is known to show variation in the frequency derivative (Perera et al. 2014). The observed trend in δDM can therefore be explained as a combined effect of both the solar wind and the varying frequency derivative.

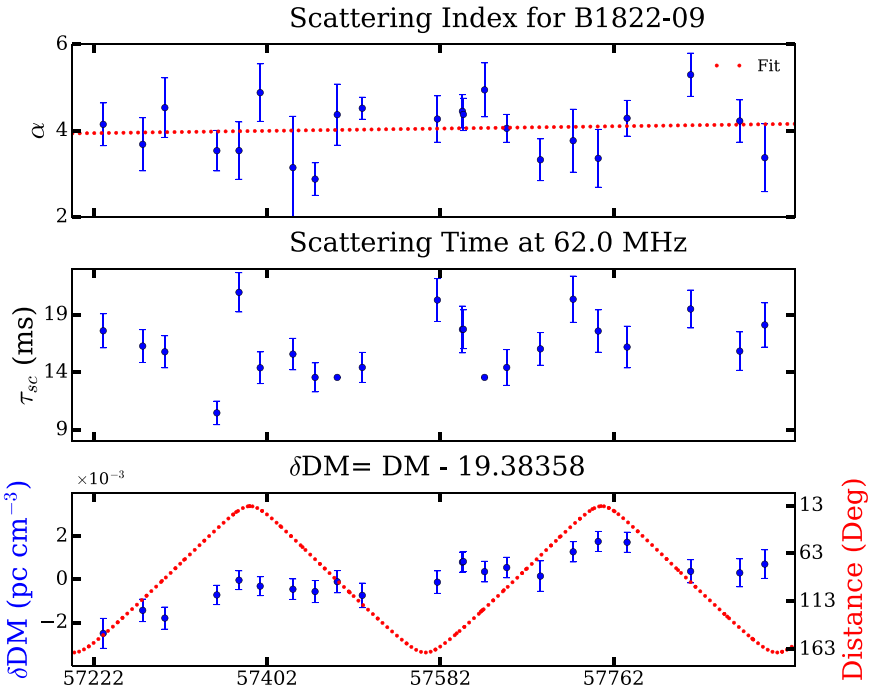

Figure 6. α, τ_{sc} at 62.0 MHz, δDM, and solar elongation angle for every epoch for PSR B1822−09.

4.4. PSR B1822−09

PSR B1822−09 is a single-component pulsar. We have obtained the frequency evolution from these four frequencies: 87, 149, 400, and 408 MHz. For this pulsar, we have reduced the data to four channels instead of two to compare our results with Krishnakumar et al. (2017; hereafter, KK17 and see Section 5.1), as they also reduced it to four channels for their analysis. We have plotted α, δDM, and relative solar distance over the observation time in Figure 6. The median α value is 4.18 ± 0.13. This value falls in the range of both the Kolmogorov and Gaussian models. The scattering index remains constant over the duration of our observations, with a slope equal to $0.11 \pm 0.25\,\mathrm{yr}^{-1}$.

PSR B1822−09 is a nearby pulsar with a DM of $19.38\,\mathrm{pc\,cm}^{-3}$ (Table 1). Its minimum solar elongation angle is about 13°. As can be seen in the Figure 6(c), there is an overall increment in the δDM value of $4.8 \times 10^{-3}\,\mathrm{pc\,cm}^{-3}$ over a span of about three years. Additionally, there are smooth rises and dips with a magnitude of 2.4×10^{-3} over a span of 167 days, which are due to changes in the solar separation angle. The transverse speed of $22\,\mathrm{km\,s}^{-1}$, implying that the LOS of this pulsar remains the same. The overall increase in δDM implies turbulence in the ISM along the LOS. Since the LOS remains the same, the scattering index remains constant.

4.5. B1839+56

PSR B1839+56 is another single-component pulsar. We have derived the IPM using 143 MHz profile. Due to poor S/N at 79.2 MHz, we were unable to obtain frequency evolution for this pulsar. We have plotted the α, δDM values, and relative solar distance for this pulsar in Figure 7. The median value of α is 2.70 ± 0.16. The α remain mostly constant, with an estimated slope of $0.10 \pm 0.05\,\mathrm{yr}^{-1}$.

The δDM values for B1839+56 are small compared (of the order of $10^{-4}\,\mathrm{pc\,cm}^{-3}$) to the other pulsars (of the order of $10^{-3}\,\mathrm{pc\,cm}^{-3}$) discussed in this paper. Also, these error bars are comparable to the variation in δDM , thus, implying insignificant variation in DM over time.

4.6. B1842+14

This is a double-component pulsar at LWA frequencies. The IPM has been obtained using the LOFAR data at 143 MHz and the LWA profile at 79.2 MHz. We only use frequency evolution of the main component as discussed in Section 3.1. We have plotted α, τ_{sc} at 69.4 MHz, δDM, and relative solar distance in Figure 8. The median α value is 3.24 ± 0.11. The α remains constant over the duration of our observations, with a fitted slope value equal to $0.09 \pm 0.12\,\mathrm{yr}^{-1}$.

From the δDM plot (Figure 8(c)), we see a moderately constant δDM until epoch MJD 57756 and a linear change of $5.8 \times 10^{-3}\,\mathrm{pc\,cm}^{-3}$ over 455 days. This does not correlate with the solar elongation angle and the closest angular distance of this pulsar to the Sun is about 37°, which is too far away to affect the DM significantly. The transverse velocity of this pulsar is about $365\,\mathrm{km\,s}^{-1}$ (Table 1), which would affect the LOS, hence, the δDM. We note that this change in LOS does not affect scattering index.

4.7. B2217+47

PSR B2217+47 is typically known to have a single component below 300 MHz (Kuzmin et al. 1998); however, recently it was found to have an additional component (Pilia et al. 2016). This component changes its relative position to the main component over time (Michilli et al. 2018). Since we do not have all the frequency data for the same epoch, we choose to ignore this component and only use the main component for IPM. We obtain the frequency evolution of the pulse component using 79.2, 143, and 151 MHz. This pulsar also has the highest S/N in our sample (Stovall et al. 2015).

For PSR B2217+47, we have plotted α values for all epochs to see if there is any variation over time (Figure 9(a)). The median α is 3.58 ± 0.10. The green dotted line represents the

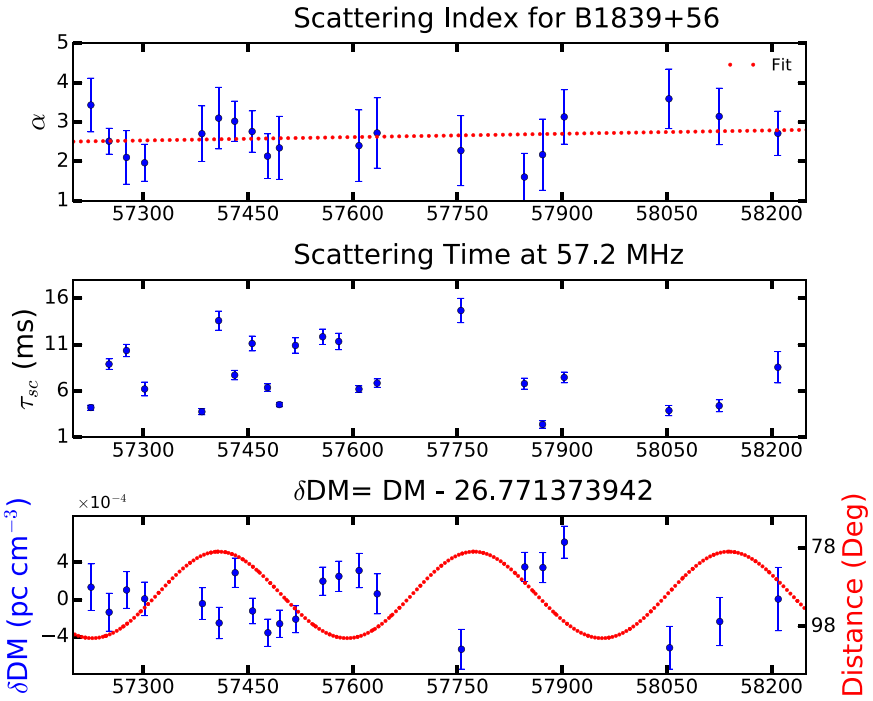

Figure 7. α, τ_{sc} at 57.2 MHz, δDM, and solar elongation angle for every epoch for B1839+56.

linear fit with an estimated slope of $-0.44 \pm 0.10\,\mathrm{yr}^{-1}$, which implies a decrement in α at a level of 4.4σ.

Figure 9(c) shows a variation in δDM values over time. The overall variation in δDM is about 0.005 pc cm^{-3} over a span of 661 days. To understand the variation in DM, we plot the solar elongation of this pulsar during our observation period (Figure 9(c)), which changes periodically, which is different from both α and δDM trends. The closest angular distance of PSR B2217+47 from the Sun is about 50°, which does not affect the pulsar DM significantly. Since both scattering index and δDM values vary with time, we test if they are correlated using Spearman rank-order correlation. We estimate the correlation index between the α and δDM values equal to -0.56 (P-value $= 0.003$), implying a negative correlation between them. We also estimate the correlation index between δDM values and scattering timescales at multiple frequencies. For the higher-frequency bands, there is a positive correlation with a similar magnitude as α, thus confirming our expectation that variation in DM affects the scattering timescale (see Equations (1) and (2)).

5. Discussion and Conclusion

We will now summarize our results and discuss what information is gained from time evolution of scattering parameters. We will also discuss how our results align with the thin-screen model and the underlying assumptions.

5.1. Scattering Spectral Index Distribution

Assuming that the scattering time follows a power law (see Equations (1) and (2)), we performed a weighted least-squares fit to estimate the spectral indices for the pulsars in our sample. Our results show that the α values, except for the two pulsars in our sample, show deviations from the theoretical power law. The scattering spectral index allows an estimate of the electron density index (β; see Equation (4)). Table 3 summarizes the scattering spectral index median value and β for our sample of pulsars. Since Equation (4) is only applicable for $\alpha > 4$, we have been able to obtain this only for PSR B0329+54 and PSR B1822−09 (see Xu & Zhang 2017 for more details).

The α measurements for PSR B0329+54 and PSR B1822−09 are consistent with the theoretical value of 4.4 for a Kolmogorov distribution. Our median α value for these pulsars slightly differs from α values of 4.3 ± 0.1 and 5.0 ± 0.5, respectively, as reported in KK17. The reason for this discrepancy is likely a different IPM. They used the 87 MHz profile with no frequency evolution for the IPM, whereas we used a higher frequency (151 MHz) with frequency evolution (refer Sections 4.3 and 4.4). We also note that assuming no frequency evolution overestimates the τ_{sc} and thus the value for α.

Among all the pulsars, PSR B0823+26 has the lowest value of α, 1.55 ± 0.40. We compare this observation with a scattering measurement done by Kuzmin & Losovsky (2007), who reported the α value for this pulsar to be 3.68 (no error bar reported). This is quite different from our observation; however, their value was obtained using only two frequencies, which makes it less reliable. Another way of obtaining a scattering spectral index is by using the spectral dependence of the decorrelation bandwidth, as done by Daszuta et al. (2013) for PSR B0823+26. The decorrelation bandwidth is related to the scattering time by $2\pi\tau_{sc}\delta\nu_d = C_1$, where ν_d is the decorrelation bandwidth. They have found this value to be 3.94 ± 0.36, which also differs significantly from our observation. However, this decorrelation bandwidth measurement is at higher frequencies (>300 MHz), which raises a question of if the scattering index varies with frequency.

Other pulsars with a large α deviation from theoretical expectations are B1839+56 and B0919+06, with estimated median values of 2.70 ± 0.16 and 2.88 ± 0.18, respectively. We compare our α measurement for B0919+06 with Kuzmin & Losovsky (2007), where they have reported a value of

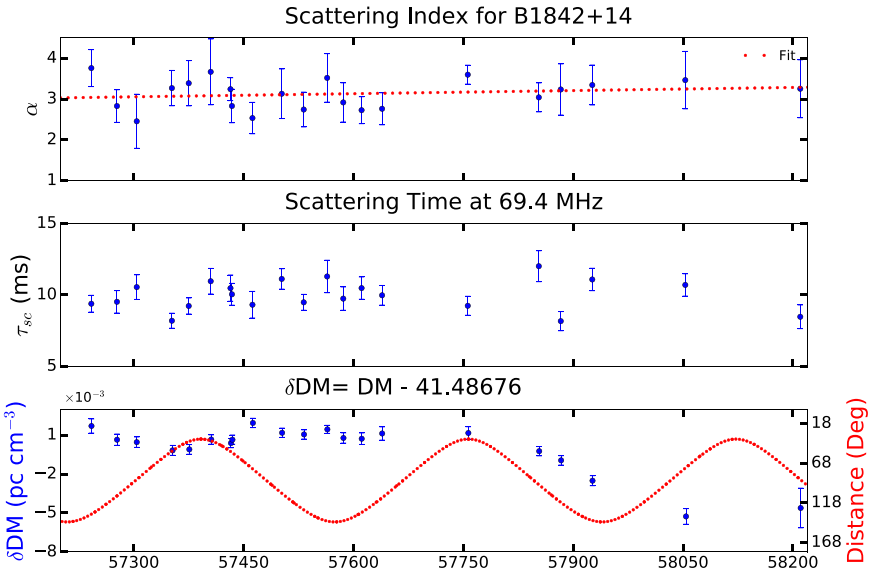

Figure 8. α, τ_{sc} at 69.4 MHz, δDM, and solar elongation angle for every epoch for B1842+14.

3.05 ± 0.08. This agrees with our measurement within the error bars, and compared to PSR B0823+26 this is likely to be more reliable because it was obtained using three frequencies.

PSR B2217+47 has a median α value of 3.58 ± 0.10. This is lower than the theoretical value for a Gaussian distribution of 4, but closer to that theoretical expectation than the α values for four pulsars in our sample. Similar to PSR B0329+54 and B1822−09, our α value for B2217+47 agrees with values reported in the literature (4.2 ± 0.1, see KK17) but is slightly higher than our median due to a different IPM. For PSR B1839 +56 and PSR B1842+14, this is the first time scattering spectral index has been estimated. In this study, we have considered no frequency evolution for three pulsars (e.g., PSR B0823+26, see Table 2) in our sample for which we suggest that the reported values should be on the higher end.

5.2. Deviation from Theoretical Models

PSR B0823+26 is the nearest source in our sample and shows large deviations in the scattering index from the thin-screen model. There are three possible explanations for this observation. First, this pulsar shows intrinsic variation such as nulling, sub-pulse drifting, and mode switching, which may affect the average profile and thus the evaluation of scattering time. This pulsar also has a small scattering time in comparison to PSR B1822−09, even though both sources have the same DM. The second explanation for this observation is that because scattering time is small in comparison to the pulse width, it is difficult to obtain the true scattering time, thus we get a flatter index. The third explanation is based on inner scale effects. At lower frequencies the diffraction scale can become smaller than the inner scale, which causes flatter spectra compared to the theoretical model. This explains the discrepancy in the observed α value with that reported in Daszuta et al. (2013), as they had observed it at a higher frequency, implying steeper spectra.

As mentioned in the introduction, deviation from the theoretical models has been observed in many scattering observations across all ranges of DM, more often for high DM pulsars (Lewandowski et al. 2013, 2015). KK17 claimed that α estimates for DMs $<50\,\mathrm{pc\,cm^{-3}}$ are in good agreement with those expected for a Kolmogorov spectrum with an average value of 3.9 ± 0.5. However, on an individual basis these sources show a deviation from the expected value.

There are various plausible explanations for these deviations. First of all, the thin-screen model assumes an infinite thin screen. This assumption seems valid in the case of medium-range DMs. For large DMs, the probability of having multiple screens increases, hence, the assumption of the thin screen becomes less valid. In the literature, most of the scattering studies (Lewandowski et al. 2013, 2015) have been conducted for high-DM pulsars (DM $> 300\,\mathrm{pc\,cm^{-3}}$), where $\alpha < 4$ have been attributed to multiple finite scattering screens. For the low-DM sources, the scattering screen can be finite, which can lead to α values less than or equal to 4.0 (Cordes & Lazio 2001). Spectra with $\alpha < 4$ are expected as a result of finite scattering screen by Rickett et al. (2009) and anisotropic scattering mechanisms by Stinebring et al. (2001).

In a recent simulation study, Geyer & Karastergiou (2016) found that for anisotropic scattering, the spectral index of scattering time is <4 with the infinite and finite screen. Anisotropy in scattering implies elongated scattering angle in one direction, compared to other directions. However, the effect of anisotropy would be more distinctive in the case of image broadening, as compared to temporal broadening. We note that in the case of PSR B2217+47, where we see a change in scattering index with time, its velocity along decl. is only 2.5 times the R.A., which makes it difficult to interpret if the observed trend is due to a change in anisotropy. We discuss this source further in more detail in Section 5.3. In order to conclusively determine the effect of anisotropy, in addition to measuring the temporal broadening, we either need to image the source simultaneously or study its dynamic spectrum. From this study, we suggest that low-DM pulsars do not always follow a Kolmogorov distribution or Gaussian distribution. This is likely due to the deviation of the scattering model from the thin-screen model even for the nearby pulsars.

Apart from DM, another important factor that will likely affect the scattering is the location of a pulsar in the Galaxy. Among the previous studies, Lewandowski et al. (2015) reported no correlation between the scattering spectral index and the distance or the position of the source in our Galaxy.

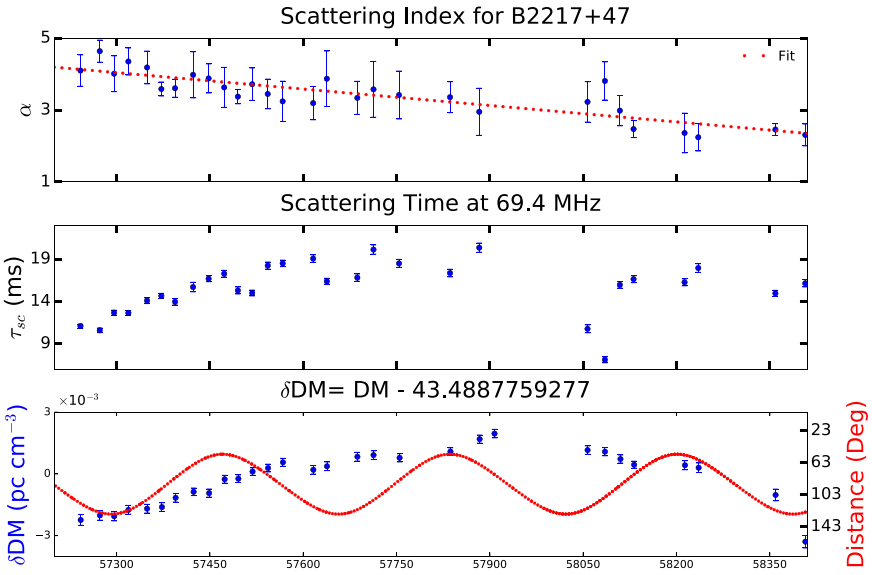

Figure 9. α, τ_{sc} at 69.4 MHz, δDM, and solar elongation angle for every epoch for B2217+47. We include scattering time to show its correlation with δDM (see Section 4.7).

Table 3
Median Values Obtained in This Study

Scattering Results		
Pulsar	α	β
B0329+54	4.05 ± 0.14	3.95
B0823+26	1.55 ± 0.09	···
B0919+06	2.83 ± 0.18	···
B1822−09	4.18 ± 0.13	3.83
B1839+56	2.70 ± 0.16	···
B1842+14	3.24 ± 0.11	···
B2217+47	3.58 ± 0.10	···

Note. α and β are scattering index and electron density index, respectively (see Equations (3) and (4)).

Similarly, KK17 did not suggest any trend in their data with respect to the location in our Galaxy and emphasized that to draw conclusions from such a plot, we need DM-independent distance measurements.

5.3. Time Evolution of Scattering Parameters

The main focus of this paper is to study the evolution of α with time, and to understand it in more detail we also obtain variation in DM in parallel for the same epochs. In our sample of seven pulsars, only B2217+47 shows a significantly varying α, whereas we see a variation in DM for all pulsars except PSR B1839+56. This variation in DM can be periodic, linear, or a combination of both depending on the underlying effects. A linear trend in DM can be explained either due to the change in LOS due to the proper motion of a pulsar or a change in distance to the screen along the LOS (Petroff et al. 2013; Lam et al. 2016). Periodic variation in DM can be attributed to either the ionosphere or the solar wind. We estimated the contribution of the ionosphere to DM, which is of the order of $<10^{-4}$ pc cm^{-3}, as about 10 times smaller than the DM variations we measured, hence it would not affect our observations. We used an IONEX Global Ionosphere Model[7] to model the slant total electron content in the ionosphere and converted that to a DM because they are the same measurement with different units. From our observations we note that solar wind will affect the DM for the slow pulsars with a minimum solar elongation of about 15°.

For PSR B0823+26, the δDM plot shows periodic variation, which is mainly due to the change in solar elongation angle. Similarly, for B1822−09, we see smooth periodic rises and dips due to changes in angular distance to the Sun, as well as an overall change of 0.001 pc cm^{-3} per year in δDM. This implies a slight variation in the column density along the LOS.

We note that we have derived these DM values from timing solutions that also depend on the intrinsic properties of a pulsar including the ISM. In such cases, the derived DM values may not represent the actual DM of the ISM. This is true for PSR B0329+54 and B0919+06 for which intrinsic variations in pulsars cause large timing residuals. The δDM plot for PSR B0329+54 shows variation in δDM; however, the actual variation is in the timing residuals due to the possibility of planets in its orbit (Starovoit & Rodin 2017). The δDM variation for B0919+06 also includes variation in pulsar frequency derivative. Since the trends in δDM for both pulsars are due to intrinsic reasons, this requires further investigation and is beyond the scope of this paper. .

We expect a change in DM due to the change in LOS to also affect the scattering spectral index. This is the case for PSR B2217+47, which shows a decrement in α values with time. The α and δDM are anti-correlated and the scattering time at higher frequencies is positively correlated with δDM (Figure 9). This pulsar is known to have an additional component, a trailing component in the main pulse (Michilli et al. 2018). However, we do not see this additional component at our frequencies. We see a similar change in DM as reported in Michilli et al. (2018) of 0.004 pc cm^{-3} over the same duration. This implies that this pulsar is encountering a gas cloud with a higher density and its structure is changing, which is affecting the pulse broadening.

We note that variations in DM may not affect the scattering spectral index if the motion is parallel to the LOS, because the ISM structure would remain the same along the LOS (Lam

[7] ftp://cddis.gsfc.nasa.gov/gnss/products/ionex/

et al. 2016). In the case of PSR B1842+14, there is a change in DM but no variation in the scattering index. This implies that this change is likely due to a change in electron density along the LOS and the structure of the ISM remains the same.

6. Summary

We present a study of the scattering spectral index and DM variation for seven pulsars over the timescale of ∼3 yr using the LWA1. This is the first time a systematic evolution of α has been reported, according to our survey of the literature. Most of the pulsars in our sample exhibit constant α throughout the observations, with the slope value consistent with zero. The exception to this is PSR B2217+47, where we measure a decrement in α over our observation period of three years, which anti-correlates with a change in DM. For PSR B0823 +26, we obtain the smallest α value of 1.55 ± 0.40, indicating inner scale effects.

The median scattering spectral index for five of the seven studied pulsars is below 4, implying deviation from both Gaussian and Kolmogorov inhomogeneities for DM <50 pc cm^{-3}. α measurements at lower frequencies and their deviations from theoretical models have led to an improved understanding of correlations between ISM structure and pulsar scattering, but the detailed structure of the ISM and the physical interpretation still remains unclear. Anisotropy is another likely explanation for these deviations in scattering spectral index. However, to effectively understand the anisotropy in the ISM, we need to study the dynamic spectra parallel to the temporal broadening for a larger sample of pulsars. More observations of other pulsars at these low frequencies will be helpful for understanding the distribution of scattering spectral index with DM. Similarly, DM-independent distance measurements will be helpful for obtaining the scattering index distribution across the Galaxy.

We thank Joe Malins for help with the ionosphere DM estimations. We also thank the anonymous referee for the valuable suggestions that improved this paper. Construction of the LWA has been supported by the Office of Naval Research under Contract N00014-07-C-0147 and by the AFOSR. Support for operations and continuing development of the LWA1 is provided by the Air Force Research Laboratory and the National Science Foundation under grants AST-1835400 and AGS1708855.

ORCID iDs

K. Bansal https://orcid.org/0000-0002-7418-7862
G. B. Taylor https://orcid.org/0000-0001-6495-7731
Kevin Stovall https://orcid.org/0000-0002-7261-594X
Jayce Dowell https://orcid.org/0000-0003-1407-0141

References

Arzoumanian, Z., Baker, P. T., Brazier, A., et al. 2018, ApJ, 859, 47
Bartel, N., Morris, D., Sieber, W., & Hankins, T. 1982, ApJ, 258, 776
Chen, J. L., Wang, H. G., Wang, N., et al. 2011, ApJ, 741, 48
Cordes, J., & Lazio, T. 2001, ApJ, 549, 997
Cordes, J., & Lazio, T. 2002, arXiv:astro-ph/0207156
Daszuta, M., Lewandowski, W., & Kijak, J. 2013, MNRAS, 436, 2492
Ellingson, S. W., Taylor, G. B., Craig, J., et al. 2013, ITAP, 61, 2540
Ferdman, R. D., van Haasteren, R., Bassa, C. G., et al. 2010, CQGra, 27, 084014
Gangadhara, R. T., & Gupta, Y. 2001, ApJ, 555, 31
Geyer, M., & Karastergiou, A. 2016, MNRAS, 462, 2587
Han, J., Han, J. L., Peng, L.-X, et al. 2016, MNRAS, 456, 3413
Kramer, M. 1994, A&AS, 107, 527
Krishnakumar, M. A., Joshi, B. C., & Manoharan, P. K. 2017, ApJ, 846, 104
Krishnakumar, M. A., Mitra, D., Naidu, A., et al. 2015, ApJ, 804, 23
Kuzmin, A. D., Izvekova, V. A., Shitov, Y. P., et al. 1998, A&AS, 127, 355
Kuzmin, A. D., & Losovsky, B. Y. 2007, A&AT, 26, 597
Lam, M. T., Cordes, J. M., Chatterjee, S., et al. 2016, ApJ, 821, 66
Lambert, H. C., & Rickett, B. J. 1999, ApJ, 517, 299
Lang, K. R. 1971, ApJ, 164, 249
Lewandowski, W., Dembska, M., Kijak, J., & Kowalinska, M. 2013, MNRAS, 434, 69
Lewandowski, W., Kowalinska, M., & Kijak, J. 2015, MNRAS, 449, 1570
Lohmer, O., Kramer, M., Mitra, D., Lorimer, D. R., & Lyne, A. G. 2001, ApJ, 562, 157
Lohmer, O., Mitra, D., Gupta, Y., Kramer, M., & Ahuja, A. 2004, A&A, 425, 569
Michilli, D., Hessels, W., & Donner, J. Y. 2018, MNRAS, 476, 2704
Perera, B. B. P., Stappers, B. W., Weltevrede, P., et al. 2014, MNRAS, 446, 1380
Petroff, E., Keith, M. J., Johnston, S., et al. 2013, MNRAS, 435, 1610
Pilia, M., Hessels, J. W. T., Stappers, B. W., et al. 2016, A&A, 586, A92
Lyne, A., Graham-Smith, F., et al. 2016, Pulsar Astronomy (Cambridge: Cambridge Univ. Press)
Rathnasree, N., & Rankin, J. M. 1995, ApJ, 452, 814
Rankin, J. M., Rodriguez, C., & Wright, G. A. E. 2006, MNRAS, 370, 673
Rickett, B. J., Johnston, S., Tomlinson, T., & Reynolds, J. 2009, MNRAS, 395, 1391
Romani, R. W., Narayan, R., & Blandford, R. 1986, MNRAS, 220, 19
Scheuer, P. A. G. 1968, Natur, 218, 920
Seiber, W. 1973, A&A, 28, 237
Shannon, R. M., Ravi, V., Lentati, L. T., et al. 2015, Sci, 349, 1522
Sobey, C., Young, N. J., Hessels, J. W. T., et al. 2015, arXiv:1505.03064v1
Standish, E. M. 1998, A&A, 336, 381
Starovoit, E. D., & Rodin, A. E. 2017, ARep, 61, 948
Stinebring, D. R., McLaughlin, M. A., Cordes, J. M., et al. 2001, ApJL, 549, L97
Stovall, K., Ray, P. S., Blythe, J., et al. 2015, ApJ, 808, 156
Taylor, G. B., Ellingson, S. W., Kassim, N. E., et al. 2012, JAI, 1, 50004
van Straten, W., Demorest, P., & Oslowski, S. 2012, AR&T, 9, 237
Williamson, I. P. 1972, MNRAS, 157, 55
Xu, S., & Zhang, B. 2017, ApJ, 835, 2
Yao, J. M., Manchester, R. N., & Wang, N. 2017, ApJ, 835, 29